Controlled mechanical properties of poly(ionic liquid)-based hydrophobic ion gels by the introduction of alumina nanoparticles with different shapes

Yuna Mizutani[a], Takaichi Watanabe[a*], Carlos G. Lopez[b], and Tsutomu Ono[a†]

[a] Department of Applied Chemistry, Graduate School of Natural Science, Okayama University, 3-1-1, Tsushima-naka,

Kita-ku, Okayama, 700-8530, JAPAN

[b] Institute of Physical Chemistry, RWTH Aachen University, 52056 Aachen, Germany, European Union

*Email: wata-t@okayama-u.ac.jp, Phone & Fax: +81-86-251-8072

†Email: tono@okayama-u.ac.jp, Phone & Fax: +81-86-251-8083

Abstract

Ionic-liquid gels, also known as ion gels, have gained considerable attention due to their high ionic conductivity and

CO_2 absorption capacity. However, their low mechanical strength has hindered their practical applications. A potential

solution to this challenge is the incorporation of particles, such as silica nanoparticles, TiO_2 nanoparticles, and metal-

organic frameworks (MOFs) into ion gels. Comparative studies on the effect of particles with different shapes are still

in progress. This study investigated the effect of the shape of particles introduced into ion gels on their mechanical

properties. Consequently, alumina/poly(ionic liquid) (PIL) double-network (DN) ion gels consisting of clustered

alumina nanoparticles with various shapes (either spherical or rod-shaped) and a chemically crosslinked poly[1-ethyl-

3-vinylimidazolium bis(trifluoromethanesulfonyl)imide] (PC_2im-TFSI, PIL) network were prepared. The results

revealed that the mechanical strengths of the alumina/PIL DN ion gels were superior to those of PIL single-network

ion gels without particles. Notably, the fracture energies of the rod-shaped alumina/PIL DN ion gels were approximately

2.6 times higher than those of the spherical alumina/PIL DN ion gels. Cyclic tensile tests were performed, and the

results revealed that the loading energy on the ion gel was dissipated through the fracture of the alumina network. TEM observation indicates the variation in the mechanical strength depending on the shape can be attributed to differences in the aggregation structure of the alumina particles, thus indicating the possibility of tuning the mechanical strength of ion gels by altering not only particle kinds but its shape.

Introduction

Ion gels are soft materials consisting of crosslinked polymer networks and a large amount of ionic liquid (IL). The IL imparts the ion gels with its intrinsic advantages (i.e. negligible vapour pressure, high thermal stability[1], flame resistance[2], high ionic conductivity[3,4], and selective CO_2 absorption capacity[5–7], while the polymer matrix enables their processability. Furthermore, the physicochemical properties of ion gels can be tailored by selecting appropriate combinations of cations and anions in the ILs[8,9]. Ion gels can be thus used in various applications, including strain sensors[10], actuators[11,12], supercapacitors[13–15], energy storage devices, and CO_2 separation membranes[7]. Moreover, employing hydrophobic polymer networks and hydrophobic ILs in ionic gels has provided these gels with excellent durability under high humidity and underwater conditions[16,17], and thus expanded their applications as separation membranes and soft electronic devices in high humidity or aquatic environments.

Like other polymer gel systems, ion gels suffer from limited mechanical stability, which limits their practical applications[18]. Significant efforts have therefore been made to develop strategies to improve the mechanical properties of ion gels. Several strategies have been proposed to enhance the mechanical strength of ion gels, such as the introduction of homogeneous crosslinked polymer networks[19–21], self-assembled ABA-type triblock copolymers[11,22], physical gelation systems using the entanglement of ultra-high molecular weight polymers[9,23], crystallisable polymer networks[24,25], and double network (DN) concepts between the polymers or between nanomaterials (fillers) and the polymer[26,27]. In particular, nanomaterial/polymer composite DN ion gels have been gaining considerable attention because toughening of the ion gels is achieved by simply adding the nanomaterials to their precursor solution.

Consequently, this approach can be applied to various monomer systems.

DN ion gels comprise two interpenetrating networks: a brittle, rigid partially clustered nanomaterial network and a soft and stretchable crosslinked polymer network. The toughening mechanism is based on energy dissipation[26]. The nanomaterial network is preferentially destroyed upon applying a large strain to the gels, which dissipates the loading energy, during which the stretchable polymer network maintains the integrity of the gel. Several studies have reported the preparation of hydrophobic DN ion gels by the introduction of various nanomaterial networks, including silica nanoparticles (NPs) [28–30], metal-organic frameworks (MOF)[31], and TEMPO-oxidised cellulose nanofibres[32]. The results of these studies revealed that the presence of hydroxyl groups on the surface of the nanomaterials is essential for the formation of nanoparticle networks in ILs and realising the toughening of ion gels. However, the relationship between the shape of nanoparticles of the brittle network and the macroscopic mechanical properties of the gels has not yet been investigated.

This paper reports the development of alumina/poly(ionic liquid) (PIL) DN ion gels composed of clustered alumina NPs with different shapes (spherical or rod-shaped) and chemically crosslinked poly[1-ethyl-3-vinylimidazolium bis(trifluoromethanesulfonyl)imide] (PC$_2$im-TFSI, PIL) networks (**Scheme 1**). The effects of the shape of the alumina NPs and their secondary network structure on the mechanical properties of the gels were also investigated. Since alumina is a well-known filler that imparts polymer composites with high heat resistance[33] and strength[34] and is expected to physically interact with IL owing to its hydroxyl groups on the surface, the rheological behaviour of the alumina (spherical or rod-shaped) /IL/ethyl acetate (EA) dispersion was investigated to confirm the formation of a physically crosslinked alumina network in the IL. Subsequently, alumina/PIL DN ion gels with varying amounts/shapes of alumina in addition to PIL single-network (SN) ion gels were prepared, and their physicochemical properties (mechanical properties, glass transition temperatures (T_g), and ionic conductivities) were compared. The ion gels were also subjected to cyclic tensile tests to evaluate their degrees of energy dissipation. The brittle network structures formed by the alumina NPs with different shapes in the IL were assessed using transmission electron

microscopy (TEM). Finally, the effects of the filler shape on the mechanical properties of ion gels were evaluated.
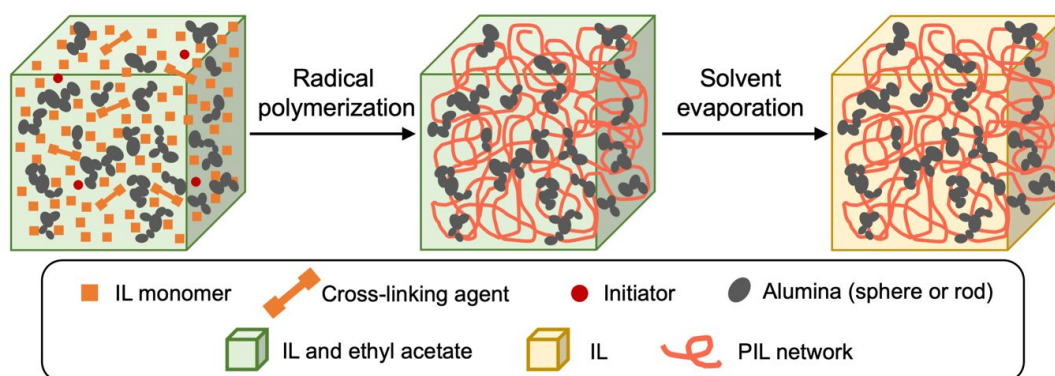
Scheme 1 Schematic illustration of the alumina/PIL DN ion gels prepared via a photo-induced radical polymerisation and subsequent solvent evaporation.

Results & discussion

To evaluate the interparticle interactions of alumina NPs in 1-butyl-3-methylimidazolium bis(trifluoromethanesulfonyl)imide ([C$_4$mim][TFSI]), the shear-rate dependencies on the viscosities of the [C$_4$mim][TFSI] solutions containing alumina of varying concentrations and shapes (spherical or rod-shaped) was investigated using a rheometer. **Figure 1** illustrates the variation in viscosity as a function of the shear rate for dispersions of spherical- and rod-shaped alumina/[C$_4$mim][TFSI]/EA at different alumina concentrations, compared with an IL/EA mixture without alumina. The results revealed that the viscosity of the IL/EA mixture was independent of the shear rate. This Newtonian behaviour is characteristic of non-structured fluids. Conversely, the alumina/[C$_4$mim][TFSI]/EA dispersions demonstrated shear thinning irrespective of the alumina shape, where the viscosity decreased with an increase in shear rate. This can be attributed to the disruption of physical bonds between the alumina NPs under shear, which is analogous to the previously reported behaviour of silica nanoparticle dispersions in IL[35,36]. For well-dispersed particles, the Einstein viscosity equation expects the zero-shear rate viscosity to increase

by only $\approx 6\%$ for the 4wt% sample. The large apparent viscosities of the solutions with alumina NPs at low shear rates

and their strong non-Newtonian character contrast with those of well-dispersed colloids[37], and give evidence of the

formation of large scale structures. This presumably occurs because the particles aggregate into clusters rather than

being individually dispersed in the solution. The spherical alumina dispersions exhibited higher low-shear viscosities

than those of the rod-shaped dispersions, which is assigned to the larger specific surface area of the spheres, enabling

the formation of a three-dimensional dendritic structure. The viscosity curves of the spherical alumina dispersions were

steeper than those of the rod-shaped dispersions, thus implying that shear forces disrupted the spherical alumina

aggregates more readily. Shear thickening was also observed in the alumina/[C$_4$mim][TFSI]/EA dispersions regardless

of the shape of alumina. The threshold shear rate at which the viscosity started to increase was in the range of 10^0–10^1

s^{-1} for spherical shapes and between 10^{-1}–100 s^{-1} for rod shapes, thus indicating that shear forces induced a pseudo-

cluster formation in rod-shaped alumina because of its higher aspect ratio which is more likely to form these clusters.

As the alumina concentration increased, the threshold shear rate decreased, thus implying a reduced possibility of shear-

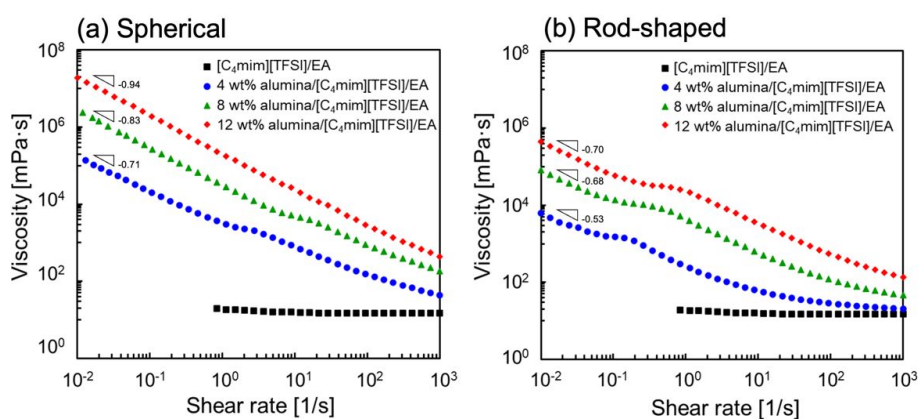induced structural breakdown of alumina with increased alumina concentrations.

Figure 1 Shear rate dependencies on the viscosities of the IL dispersions of different concentrations of (a) spherical and

(b) rod-shaped alumina.

Alumina/PIL DN ion gels with varying alumina concentration/shapes, in addition to PIL SN ion gels were prepared. The PIL DN ion gels, consisting of alumina NPs and cross-linked PC_2im-TFSI, were prepared via the photo-induced radical polymerization of 1-ethyl-3-vinylimidazolium bis(trifluoromethanesulfonyl)imide ([C_2vim][TFSI]) in a mixture containing alumina, [C_4mim][TFSI] (as ionic liquid), 1,4-bis(3-vinylimidazolium-1-yl) butane bis(trifluoromethanesulfonyl)imide ([$(Vim)_2C_4$][TFSI]$_2$, as ionic liquid cross-linker), Irgacures 2959 (as the photoinitiator), and EA (as the solvent). EA was then removed by solvent evaporation. PIL SN ion gels were prepared using a similar method but without the addition of alumina.

Figure 2 displays the photographs of the prepared ion gels. The PIL SN ion gel was found to be highly transparent with a light orange colour (**Figure 2a**), while the alumina/PIL DN ion gels were translucent white (**Figure 2b, 2c**). The incorporation of alumina resulted in a cloudy appearance of the ion gel, thus indicating that alumina NPs tended to form microscale aggregates within the ion gels. The rod-shaped alumina tended to be less transparent than the spherical alumina NPs, thus indicating that larger aggregates were formed in the ion gels containing rod-shaped alumina NPs.

TEM observations of thin sections of the gels were conducted to assess the structure of the alumina aggregates within the ion gel. **Figure 3** presents the TEM images of cross-sections of the alumina/PIL DN ion gels, where the dark-coloured particles represent the alumina NPs. The TEM images of the ion gels with spherical alumina revealed that the primary particles of alumina formed clusters (**Figure 3a**), while those of the rod-shaped alumina were aligned in parallel to form primary and secondary aggregates (**Figure 3b**). The aggregate structures formed by the spherical and rod-shaped particles within the ion gels were thus significantly different.
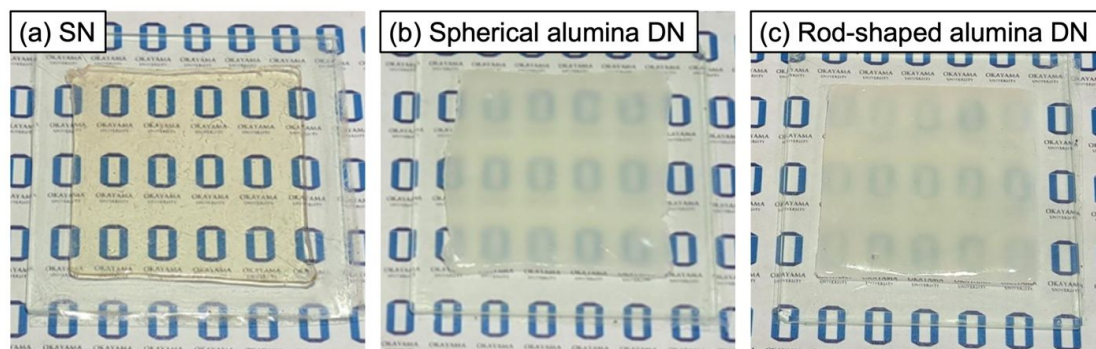
Figure 2 Photos of the PIL ion gels (a: SN, b: spherical alumina DN, c: rod-shaped alumina DN).
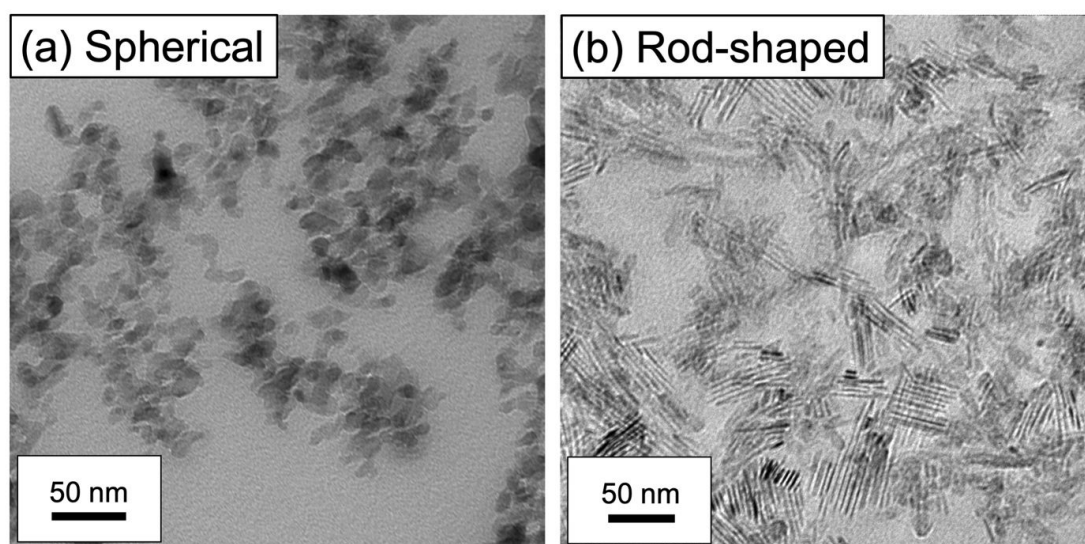

Figure 3 TEM images of the PIL ion gels with (a) spherical and (b) rod-shaped alumina.

Figure 4 shows the stress–strain curves for the spherical alumina/PIL DN ion gels and rod-shaped alumina/PIL DN ion gels with different alumina contents. The stress–strain curves of the PIL ion gel comprising 47 wt% PC_2im-TFSI and 53 wt% $[C_4mim][TFSI]$ (i.e. an alumina concentration of 0 wt%) are also provided. The results revealed that the mechanical strengths of the alumina/PIL DN ion gels were higher than those of the PIL SN ion gel, regardless of the alumina particle shape. The mechanical properties of the spherical alumina/PIL DN ion gels and rod-shaped alumina/PIL DN ion gels are shown in **Figure 5**. The results revealed that the fracture strains, stresses, and

7

energies in addition to Young's moduli tended to increase with an increase in the spherical alumina concentration (**Figure 5a**). The increase in the fracture stress and Young's modulus can be attributed to the increase in network density of dendritic structure formed by alumina with an increase in alumina concentration. Regarding the fracture strain, the dendric alumina network could mitigate the stress concentration in the PIL network and prevent it from breaking. It was hypothesised that there is a maximum effective alumina network amount for strength enhancement due to the negligible difference between the fracture energies at 12 and 14 wt%.

Figure 4b and **Figure 5b** also revealed that the Young's moduli of the rod-shaped alumina/PIL DN ion gels increased with an increase in alumina concentration, thus indicating that the rod-shaped alumina stiffened the ion gels. Although the fracture strain remained almost constant, the fracture stress increased with an increase in alumina concentration up to 10 wt%. At alumina concentrations exceeding 10 wt%, the fracture strain decreased, and the fracture stress remained almost constant. This behaviour can be attributed to the formation of large aggregates due to the excess of alumina in the IL, which introduced critical cracks thus resulting in the breakage of ion gels during stretching. The fracture energy increased with an increase in alumina concentration up to 10 wt% but then tended to decrease at higher concentrations, thus indicating a toughness threshold, even in the case of rod-shaped alumina.

The oscillatory shear temperature-sweep viscoelasticity measurements were performed to determine T_g of ion gels. T_g was identified by the temperature corresponding to the peak top of tan δ [38]. These measurements indicate that the addition of alumina to ion gels only affected their T_g (–22.6–27.3 °C) weakly, as shown in **Figure S3**. The ionic conductivities of the ion gels were also assessed using an impedance analyser. The results revealed that the introduction of alumina into the ion gels did not alter the ionic conductivities, which remained at approximately 10^{-3} S/cm at 30 °C, as illustrated in **Figure S4**. Consequently, we assumed that the enhanced mechanical strength of the ion gels containing alumina NPs was attributed to the changes in their network structure rather than their chemical properties.
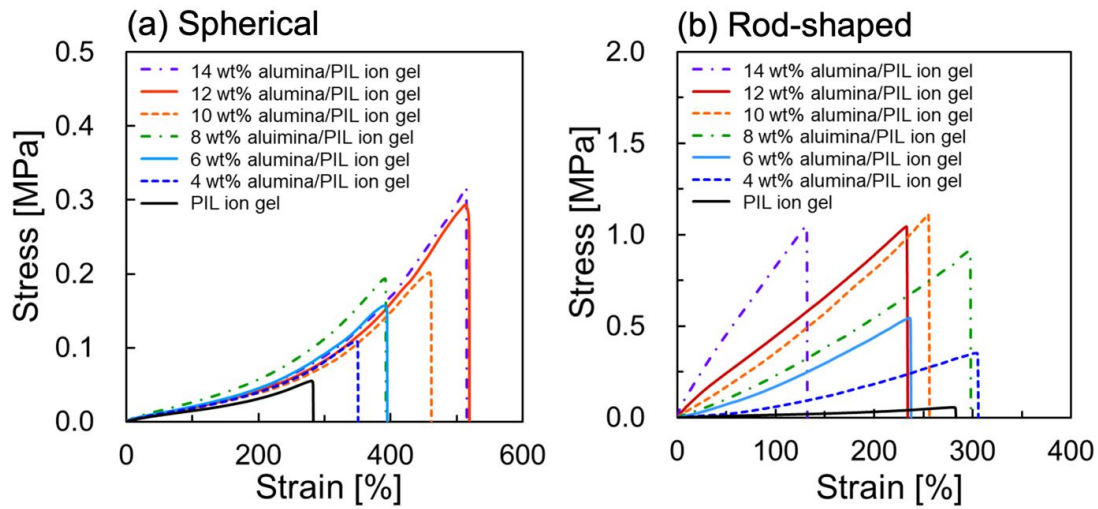
Figure 4 Stress–strain curves of (a) spherical and (b) rod-shaped alumina/PIL DN ion gels with different alumina concentrations.
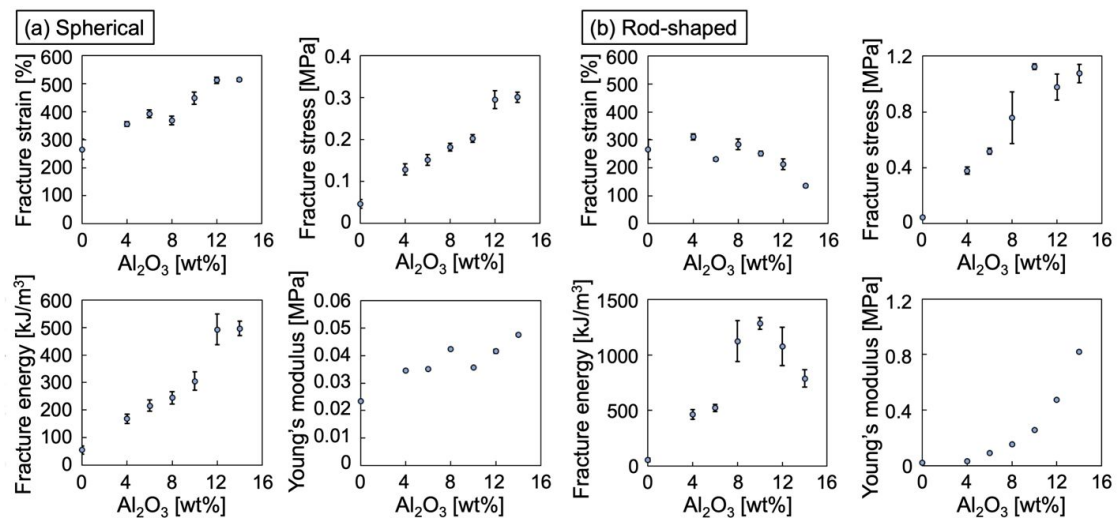

Figure 5 Mechanical properties of (a) spherical and (b) rod-shaped alumina/PIL DN ion gels with different alumina concentration.

To elucidate the toughening mechanism of the ion gel upon the addition of alumina, cyclic tensile stress loading–unloading experiments were conducted for the PIL SN ion gel, spherical alumina/PIL DN ion gels, and rod-shaped alumina/PIL DN ion gels, as shown in **Figure 6**. Regardless of the alumina shape, the alumina/PIL DN ion gels exhibited distinct hysteresis loops in the cyclic stress–strain curves, showing a softening behaviour of the ion gel when

9

loading was applied (**Figure 6b** and **6c**), whereas the PIL SN ion gel did not exhibit such behaviour (**Figure 6a**). The hysteresis loop observed in the stress–strain curve of the alumina/PIL DN ion gel can be attributed to the partial destruction of the alumina aggregates when subjected to loading, which is in accordance with the previously reported behaviour of silica NPs/PIL DN ion gels[30]. These observations strongly confirmed that the toughening mechanism in the alumina/PIL DN ion gel is attributed to energy dissipation stemming from the fracture of the alumina aggregate under a large strain.

To compare the difference in the degree of energy dissipation by spherical and rod-shaped alumina, we calculated the energy dissipation per strain cycle during the cyclic tensile stress loading-unloading experiments, as shown in **Figure 7**. The dissipated energy tended to increase with an increase in the number of cycles, irrespective of the alumina shape, thus indicating that the alumina network contributed to sustaining the loaded stress until the high-elongation state[28]. For the spherical alumina/PIL DN ion gel, the variation in the dissipated energy per cycle as a function of the concentration was minimal, while they were positively correlated in the case of the rod-shaped alumina/PIL DN ion gel. These results indicated that in the case of spherical alumina, the dendritic structure could develop with an increase in alumina concentration, whereas in the case of rod-shaped alumina, the size and the number of alumina aggregates could increase with an increase in alumina concentration.

Ion gels with rod-shaped alumina exhibited higher fracture stresses and Young's moduli, but lower fracture strains than those with spherical alumina. In the case of spherical alumina, the dendritic alumina network spread throughout the gel contributes to an increase in fracture stresses and Young's moduli without hindering the elongation of the PIL when the ion gels are stretched. Conversely, rod-shaped alumina could form large aggregates, significantly increasing fracture stresses and Young's moduli. However, the breakage of these aggregates tends to facilitate crack propagation within the gel, resulting in reduced fracture strains. Overall, the difference in mechanical strength appeared to be governed by the distinctive network structures formed within the ion gel based on the alumina shape.
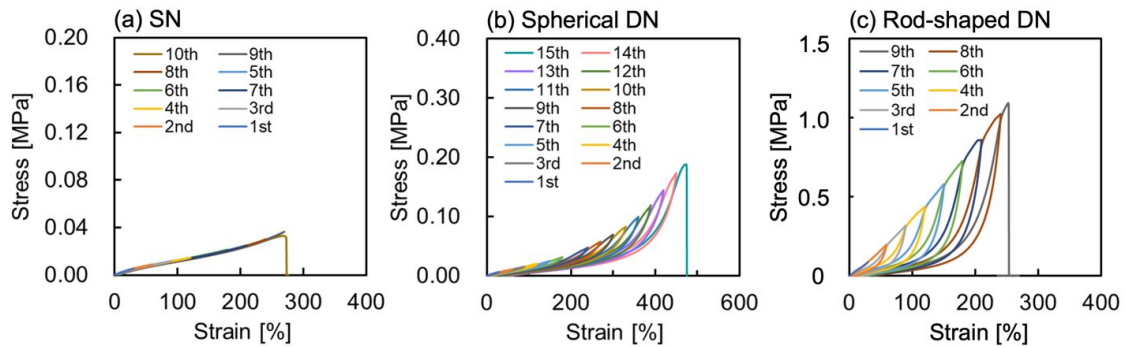
Figure 6 Cyclic tensile tests of (a) PIL SN, (b) spherical alumina/PIL DN, and (c) rod-shaped alumina/PIL DN ion gels.
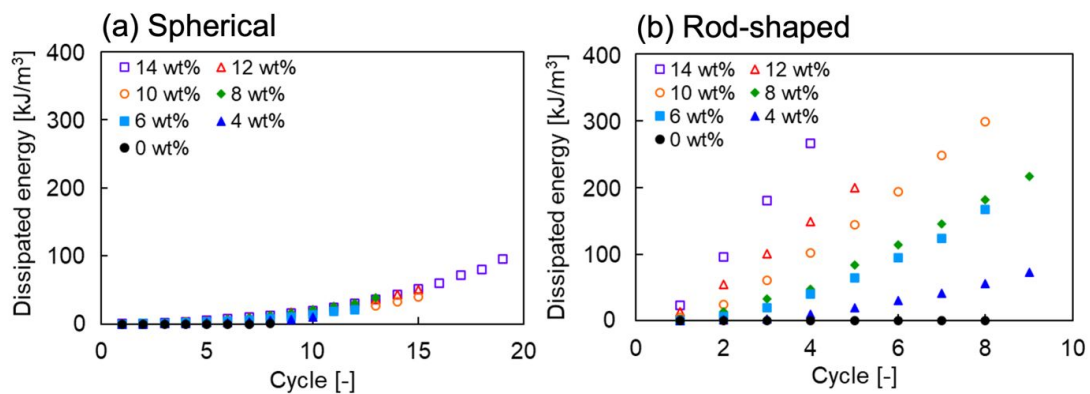

Figure 7 Dissipated energy of (a) spherical alumina/PIL DN and (b) rod-shaped alumina/PIL DN ion gels, as a function of cycle.

Conclusions

This study investigated the effect of the alumina shape on the mechanical properties of synthesized alumina/PIL DN ion gels. The results revealed that both spherical and rod-shaped alumina NPs significantly improved the mechanical strength of ion gels, although noticeable differences were attributed to the shapes of the nanoparticles, which influenced the structure of the alumina network. Spherical alumina led to a more consistent increase in the mechanical properties across different concentrations, similar to the previously reported results for silica NPs, while the rod-shaped alumina led to a stiffer ion gel and demonstrated a threshold for toughness improvement with diminishing returns beyond a specific concentration owing to the formation of large aggregates. The critical influence of the shape of the alumina on

1

the macroscopic mechanical properties of the ion gels was evident, thus underscoring the necessity of optimising the nanoparticle shape and secondary aggregation structure for specific applications. The cyclic tensile tests and rheological behaviour analysis provided insights into the toughening mechanism of the ion gels and highlighted the role of energy dissipation through the partial destruction of alumina aggregates under strain. This behaviour is consistent with the DN principle, thus validating the effectiveness of the nanomaterial/polymer composite approach for enhancing the mechanical resilience of ion gels. In summary, we found that the complex interplay between the shape of the nanomaterials and macroscopic properties of ion gels, thus providing a pathway for the rational design of ion gels with tailored mechanical properties. Future work should delve deeper into optimising the nanoparticle characteristics and explore additional nanomaterials to expand the application range and performance of ion gels.

Experimental section

Materials

Spherical alumina NPs (13 nm) were purchased from Tokyo Chemical Industry Co., Ltd. (Tokyo, Japan). Rod-shaped alumina dispersion (10 wt%) in EA was kindly provided by Kawaken Fine Chemical Co., Ltd. The minor and major axes were 10 and 50 nm, respectively. The ionic liquid, $[C_4mim][TFSI]$, ionic liquid monomer $[C_2vim][TFSI]$, 1-vinylimidazole, 1,4-dibromobutane ethanol, diethyl ether, and lithium bis(trifluoromethanesulfonyl)imide (LiTFSI) were purchased from FUJIFILM Wako Pure Chemical Corp. (Osaka, Japan) and used as received. Furthermore, 2-hydroxy-40-(2-hydroxyethyl)-2-methylpropiophenone (Ciba® IRGACURE® 2959), purchased from Ciba Specialty Chemicals (Switzerland), was used as a photoinitiator to synthesize the PC_2im-TFSI network in an IL. Dimethyl sulfoxide-d_6 was purchased from Sigma-Aldrich (Germany) and used as received. The deionised water used in all experiments was produced using an Elix UV purification system (Millipore, Japan). The chemical structures of $[C_4mim][TFSI]$, $[C_2vim][TFSI]$, Ciba® IRGACURE® 2959, $[(Vim)_2C_4]Br_2$, and $[(Vim)_2C_4][TFSI]_2$ are shown in **Figure S1** (ESI†).

Synthesis of [(Vim)$_2$C$_4$][TFSI]$_2$ as a cross-linking reagent containing ionic liquid groups

The cross-linking reagent, [(Vim)$_2$C$_4$][TFSI]$_2$, containing ionic liquid groups, was synthesised by reacting 1-vinylimidazole with 1,4-dibromobutane, followed by an anion exchange reaction with LiTFSI (**Scheme S1**, ESI†). In a round-bottom flask (300 mL) that had been dried and purged with argon, 1-vinylimidazole (0.20 mol, 18.1 mL) was dissolved in ethanol (15.0 mL). Subsequently, 1,4-dibromobutane (0.11 mol, 13.6 mL) was added dropwise to the flask and the mixture was stirred at 70 °C under an argon atmosphere for 24 h. The reaction mixture was precipitated thrice in ethyl acetate (300 mL) to remove any unreacted reagents. The purified product was dried at 50 °C under reduced pressure over night, to obtain [(Vim)$_2$C$_4$]Br$_2$ (30.2 g, yield: 75% according to the proton nuclear magnetic resonance (¹H NMR) spectrum in **Figure S2a** (ESI†). The anion exchange reaction of [(Vim)$_2$C$_4$]Br$_2$ with LiTFSI was then performed by mixing an aqueous solution (60 mL) containing [(Vim)$_2$C$_4$]Br$_2$ (7.4 mmol, 3.00 g) with another aqueous solution (60 mL) containing LiTFSI (16.5 mmol, 4.73 g). The resulting mixture was stirred at room temperature for 24 h under an argon atmosphere to exchange the Br$_2$ counter anion with the [TFSI]$_2$ anions. The resulting [(Vim)$_2$C$_4$][TFSI]$_2$ was washed thrice with pure water (100 mL) and freeze-dried for 24 h to remove any residual salt and obtain [(Vim)$_2$C$_4$][TFSI]$_2$ (4.7 g, yield: 78.5% according to the ¹H NMR spectrum in **Figure S2b** (ESI†)). The successful anion exchange from Br to TFSI was confirmed by the shift in peak from a' (9.46 ppm, 2H in **Figure S2a**, ESI†) to a (9.40 ppm, 2H in **Figure S2b**, ESI†).

Rheological measurements of the alumina/[C$_4$mim][TFSI] dispersion

The alumina/[C$_4$mim][TFSI]/EA dispersions were prepared according to the following procedure which uses as an example an alumina concentration of 4 wt%. The spherical alumina NPs (0.12 g), [C$_4$mim][TFSI] (3.5 g), and EA (1.2 mL) were mixed using a vortex mixer to obtain a homogeneous spherical alumina/[C$_4$mim][TFSI]/EA dispersion. Ten wt% rod-shaped alumina dispersion in EA (1.2 g) was mixed with [C$_4$mim][TFSI] (3.5 g) using a vortex mixer, and

then dried under reduced pressure with stirring to evaporate the excess EA. The appropriate amount of EA was added

to bring the total EA volume to 1.2 mL, and uniform rod-shaped alumina/[C$_4$mim][TFSI]/EA dispersions were prepared.

The amounts of reagent for other alumina concentrations are listed in **Table S1** and **Table S2** (ESI†). Viscosities of the

alumina/[C$_4$mim][TFSI]/EA dispersions were measured using a controlled stress rheometer (MCR302, Anton Paar,

Japan). The viscosity dependence of the shear of the alumina/[C$_4$mim][TFSI]/EA dispersion as a sample was evaluated

using a rheometer with a parallel-plate geometry (PP50; diameter = 50 mm, gap = 0.3 mm) at 25 °C. Similar

measurements were conducted by employing [C$_4$mim][TFSI] as the control. After pre-shearing at 1000 s^{-1} for 60 s, the

change in viscosity of the solution was measured as a function of shear rate from 1,000 to 0.01 s^{-1} and then from 0.01

to 1,000 s^{-1}. The limiting torque on the MCR302 rheometer is approximately 0.5 μN·m; data corresponding to torque

values below this limit was trimmed.

Preparation of the alumina/PIL DN ion gels

Alumina/PIL DN ion gels were prepared via the photopolymerization of an ionic liquid monomer ([C$_2$vim][TFSI]) in

the presence of the ionic liquid ([C$_4$mim][TFSI]), EA, and alumina. The alumina/PIL DN ion gels were prepared

according to the following procedure which uses as an example an alumina concentration of 10 wt%. To prepare

spherical alumina/PIL DN ion gels, alumina NPs (0.30 g) and [C$_4$mim][TFSI] (3.5 g) were mixed in a vortex mixer. In

the case of using rod-shaped alumina, 10 wt% rod-shaped alumina dispersion in EA (3.0 g) was mixed with

[C$_4$mim][TFSI] (3.5 g) using a vortex mixer, and then dried under reduced pressure with stirring to remove the excessive

EA. [C$_2$vim][TFSI] (3.0 g) as a monomer, [(Vim)$_2$C$_4$][TFSI]$_2$ (0.021 g) as a crosslinking agent, Irgacure 2959 (0.0016

g) as a photoinitiator, and EA (total volume 1.2 mL) were then added, mixed using a vortex mixer, and stirred to prepare

the precursor solution. The amounts of reagent for other alumina concentrations are listed in **Table S3** and **Table S4**

(ESI†). The precursor solution was injected into a mould composed of two glass plates with an FEP film and a PTFE

spacer with 1-mm thickness and was irradiated with 365 nm UV light for 13 h (1,820 μW/cm²). The product was dried

1

in vacuum at 40 °C for more than 3 h to remove EA. The IL concentration after drying was fixed at 53 wt%.

Measurement of the mechanical properties

The mechanical properties of the ion gels were evaluated using an automatic recording universal testing instrument (EZ Test EZ-SX 500 N, Shimadzu Co., Japan) at 25 °C. Dumbbell-shaped specimens with lengths, widths, and thicknesses of 35, 2, and 1 mm, respectively, were used for the tensile tests. The fabricated sample was attached to the instrument at 15 mm between the jigs. The uniaxial stretching test was conducted by stretching the sample at a constant strain rate of 50 mm min^{-1}. The stress–strain curves were recorded automatically until the specimens broke. The fracture stresses, strains, and energies in addition to the Young's moduli of the ion gels were obtained as mean values of triplicate measurements for each sample. In the cyclic tensile test, loading and unloading operations were performed, and the stress–strain curves were recorded until the sample broke while gradually increasing the stretching strain at intervals of 0.3.

Oscillatory shear temperature sweep viscoelasticity measurement of alumina/PIL DN ion gels

Temperature-sweep viscoelasticity measurements of the ion gels were performed with a parallel-plate geometry (PP25; diameter = 25 mm, gap = 1 mm) using a controlled stress rheometer (MCR302, Anton Paar, Japan). The measurements were performed in the temperature range of −80 to 160 °C, a frequency of 1 Hz, and a strain of 0.1%. T_g was determined as the temperature at the peak top of tanδ.

TEM observations of alumina/PIL DN ion gel

To confirm the morphology of alumina in the PIL ion gel, the samples were observed by a TEM (JEM-2100F, JEOL). A cubic sample of the ion gel (1 mm in size) was immersed in a sufficient amount of EA for 24 h to exchange the [C$_4$mim][TFSI] in the sample by EA. The sample was then immersed in a mixture of a precursor solution of UV-curable

resin and EA (1/1, w/w) for 24 h, followed by immersion in a precursor solution of UV-curable resin for 12 h to completely exchange the EA for the precursor solution. The sample in the precursor solution was poured into a silicon mould and cured under a UV light ($\lambda = 365$ nm) for 1 h. The resin block embedded in the gel was then thin-sectioned using an ultramicrotome (UC7, Leica Microsystems GmbH, Germany), and 100 nm-thick sections were collected on a copper mesh TEM grid. The sample was observed using TEM at an electron gun acceleration voltage of 100 kV.

Author Information

Corresponding author

E-mail: wata-t@okayama-u.ac.jp. Tel: +81-86-251-8072. Fax: +81-86-251-8072.

E-mail: tono@okayama-u.ac.jp. Tel: +81-86-251-8083. Fax: +81-86-251-8083.

ORCID

Yuna Mizutani: 0009-0006-1777-8144

Takaichi Watanabe: 0000-0002-5855-2583

Carlos G. Lopez: 0000-0001-6160-632X

Tsutomu Ono: 0000-0002-2880-7119

Conflicts of Interest

There are no conflicts to declare.

Author Contributions

Y.M., T.W., C.G.L., and T.O. designed the experiments. Y.M. and T.W. performed the experiments and analysed the data. Y.M., T.W., C.G.L., and T.O. interpreted the results and wrote the manuscript. T.W. and T.O designed the research.

Acknowledgments

References

1   Y. Wang, Y. Chen, J. Gao, H. G. Yoon, L. Jin, M. Forsyth, T. J. Dingemans and L. A. Madsen, *Adv. Mater.*, 2016, **28**, 2571–2578.

2   D. M. Fox, J. W. Gilman, A. B. Morgan, J. R. Shields, P. H. Maupin, R. E. Lyon, H. C. De Long and P. C. Trulove, *Ind. Eng. Chem. Res.*, 2008, **47**, 6327–6332.

3   J. Zhang, E. Kamio and A. Matsuoka, *Ind. Eng. Chem. Res.*, 2022, **61**, 4648–4658.

4   M. G. Cowan, D. L. Gin and R. D. Noble, *Acc. Chem. Res.*, 2016, **49**, 724–732.

5   B. E. Gurkan, J. C. de la Fuente, E. M. Mindrup, L. E. Ficke, B. F. Goodrich, E. A. Price, W. F. Schneider and J. F. Brennecke, *J. Am. Chem. Soc.*, 2010, **132**, 2116–2117.

6   W. He, F. Zhang, Z. Wang, W. Sun, Z. Zhou and Z. Ren, *Ind. Eng. Chem. Res.*, 2016, **55**, 12616–12631.

7   J. E. Bara, E. S. Hatakeyama, D. L. Gin and R. D. Noble, *Polym. Adv. Technol.*, 2008, **19**, 1415–1420.

8   S. P. M. Ventura, A. M. M. Gonçalves, T. Sintra, J. L. Pereira, F. Gonçalves and J. A. P. Coutinho, *Ecotoxicology*, 2013, **22**, 1–12.

9   Y. Kamiyama, R. Tamate, K. Fujii and T. Ueki, *Soft Matter*, 2022, **18**, 8582–8590.

10   H. Wang, Z. Wang, J. Yang, C. Xu, Q. Zhang and Z. Peng, *Macromol. Rapid Commun.*, 2018, e1800246.

11   S. Imaizumi, H. Kokubo and M. Watanabe, *Macromolecules*, 2012, **45**, 401–409.

12   X. Liu, B. He, Z. Wang, H. Tang, T. Su and Q. Wang, *Sci. Rep.*, 2014, **4**, 6673.

13   X. Yang, F. Zhang, L. Zhang, T. Zhang, Y. Huang and Y. Chen, *Adv. Funct. Mater.*, 2013, **23**, 3353–3360.

14   T. Y. Kim, H. W. Lee, M. Stoller, D. R. Dreyer, C. W. Bielawski, R. S. Ruoff and K. S. Suh, *ACS Nano*, 2011, **5**, 436–442.

15   S. Hong, Y. Yuan, C. Liu, W. Chen, L. Chen, H. Lian and H. Liimatainen, *J. Mater. Chem.*, 2020, **8**, 550–560.

16   Y. J. Son, J. W. Bae, H. J. Lee, S. Bae, S. Baik, K.-Y. Chun and C.-S. Han, *J. Mater. Chem. A Mater. Energy Sustain.*, 2020, **8**, 6013–6021.

17   L. Rong, X. Xie, W. Yuan and Y. Fu, *ACS Appl. Mater. Interfaces*, 2022, **14**, 29273–29283.

18   C. S. Patrickios and K. Matyjaszewski, *Polym. Int.*, 2021, **70**, 10–13.

19   S. Ishii, H. Kokubo, K. Hashimoto, S. Imaizumi and M. Watanabe, *Macromolecules*, 2017, **50**, 2906–2915.

20   H. Asai, K. Fujii, T. Ueki, T. Sakai, U.-I. Chung, M. Watanabe, Y.-S. Han, T.-H. Kim and M. Shibayama, *Macromolecules*, 2012, **45**, 3902–3909.

21   K. Fujii, H. Asai, T. Ueki, T. Sakai, S. Imaizumi, U.-I. Chung, M. Watanabe and M. Shibayama, *Soft Matter*, 2012, **8**, 1756–1759.

22   R. Tamate, K. Hashimoto, T. Horii, M. Hirasawa, X. Li, M. Shibayama and M. Watanabe, *Adv. Mater.*, 2018, **30**,

1–7.

23   Y. Kamiyama, R. Tamate, T. Hiroi, S. Samitsu, K. Fujii and T. Ueki, *Sci Adv*, 2022, **8**, eadd0226.

24   W. Li, L. Li, Z. Liu, S. Zheng, Q. Li and F. Yan, *Adv. Mater.*, 2023, **35**, e2301383.

25   M. Wang, P. Zhang, M. Shamsi, J. L. Thelen, W. Qian, V. K. Truong, J. Ma, J. Hu and M. D. Dickey, *Nat. Mater.*, 2022, **21**, 359–365.

26   J. P. Gong, Y. Katsuyama, T. Kurokawa and Y. Osada, *Adv. Mater.*, 2003, **15**, 1155–1158.

27   J. P. Gong, *Soft Matter*, 2010, **6**, 2583–2590.

28   T. Yasui, E. Kamio and H. Matsuyama, *Langmuir*, 2018, **34**, 10622–10633.

29   T. Yasui, S. Fujinami, T. Hoshino, E. Kamio and H. Matsuyama, *Soft Matter*, 2020, **16**, 2363–2370.

30   T. Watanabe, R. Takahashi and T. Ono, *Soft Matter*, 2020, **16**, 1572–1581.

31   E. Kamio, M. Minakata, H. Nakamura, A. Matsuoka and H. Matsuyama, *Soft Matter*, 2022, **18**, 4725–4736.

32   T. Watanabe, E. Oe, Y. Mizutani and T. Ono, *Soft Matter*, 2023, **19**, 2745–2754.

33   C. Zeng, S. Lu, L. Song, X. Xiao, J. Gao, L. Pan, Z. He and J. Yu, *RSC Adv.*, 2015, **5**, 35773–35782.

34   Z. Guo, T. Pereira, O. Choi, Y. Wang and H. Thomas Hahn, *J. Mater. Chem.*, 2006, **16**, 2800–2808.

35   K. Ueno, K. Hata, T. Katakabe, M. Kondoh and M. Watanabe, *J. Phys. Chem. B*, 2008, **112**, 9013–9019.

36   K. Ueno, *Polym. J.*, 2018, **50**, 951–958.

37   A. Scotti, M. Brugnoni, C. G. Lopez, S. Bochenek, J. J. Crassous and W. Richtering, *Soft Matter*, 2020, **16**, 668–678.

38   K. Sakurai, T. Maegawa and T. Takahashi, *Polymer*, 2000, **41**, 7051–7056.

Electronic Supplementary Information (ESI) for

Controlled mechanical properties of poly(ionic liquid)-based hydrophobic ion gels by the introduction of alumina nanoparticles with different shapes

Yuna Mizutani[a], Takaichi Watanabe[a*], Carlos G. Lopez[b], and Tsutomu Ono[a†]

[a] Department of Applied Chemistry, Graduate School of Natural Science, Okayama University, 3-1-1, Tsushima-naka, Kita-ku, Okayama, 700-8530, JAPAN

[b] Institute of Physical Chemistry, RWTH Aachen University, 52056 Aachen, Germany, European Union

[*]Email: wata-t@okayama-u.ac.jp, Phone & Fax: +81-86-251-8072

[†]Email: tono@okayama-u.ac.jp, Phone & Fax: +81-86-251-8083

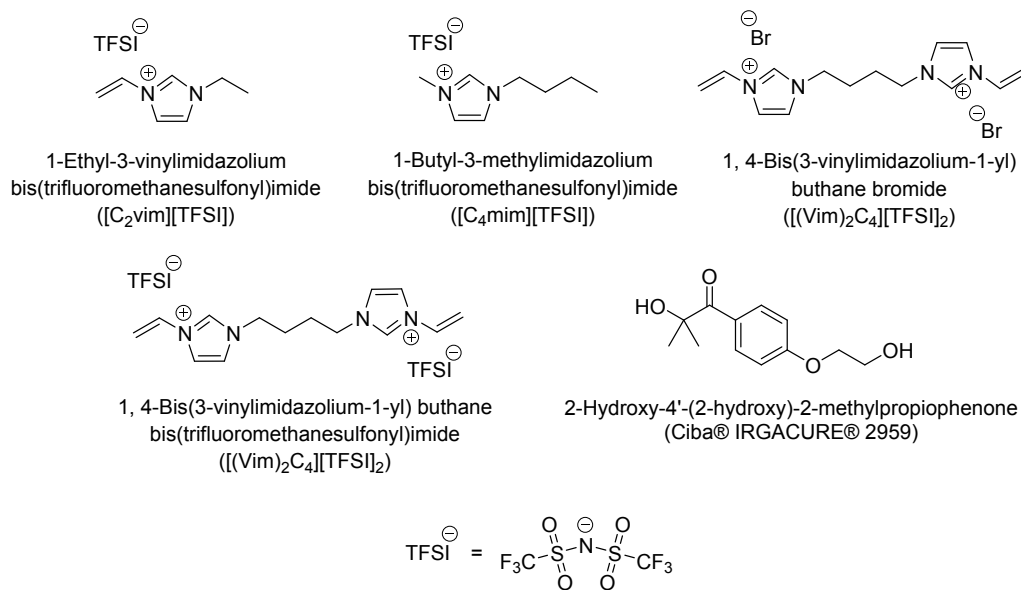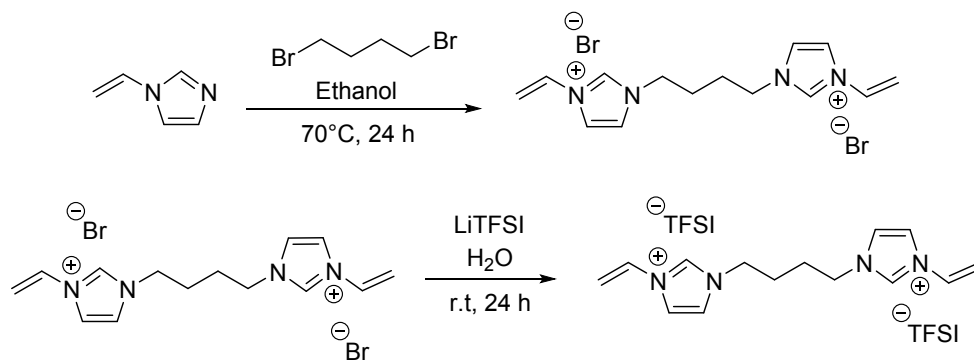Keywords: Ion gel, Composite, Double network, Dissipation, Toughening

Figure S1 Chemical structures of reagents used for preparing PIL ion gels.

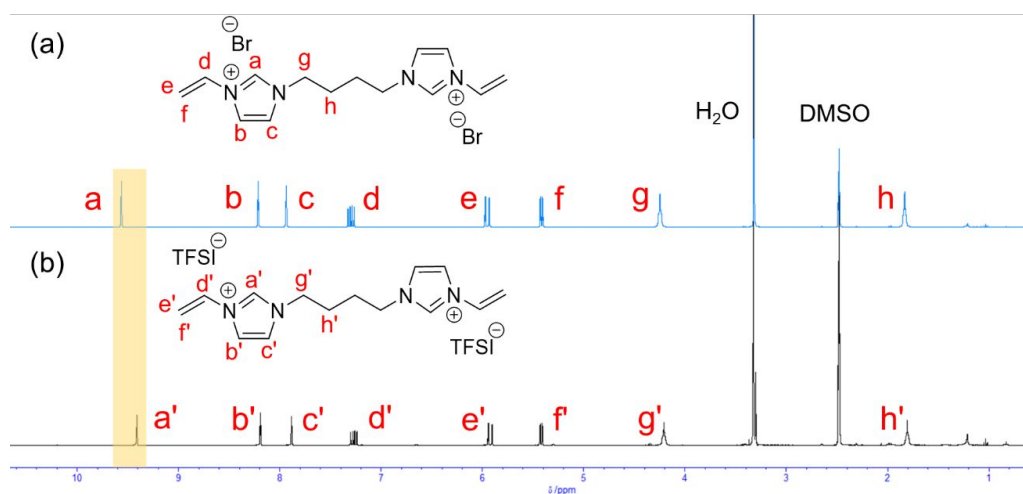**Scheme S1** Synthesis of [(Vim)₂C₄]Br₂ and [(Vim)₂C₄][TFSI]₂

Figure S2 ^{1}H NMR spectra of (a) $[(Vim)_2C_4]Br_2$ and (b) $[(Vim)_2C_4][TFSI]_2$. (Solvent: DMSO-d_6).

Table S1 Amount of reagent used for spherical alumina/$[C_4mim][TFSI]$/Ethyl acetate (EA) dispersion.

IL $[C_4mim][TFSI]$	Total EA	Alumina		
[g]	[mL]	[g]	[wt%]*^{1}	[vol%]*^{2}
3.5	1.2	0.12	4.1	0.84
3.5	1.2	0.24	7.9	1.6
3.5	1.2	0.36	12	2.5

*^{1} Alumina [wt%] corresponds to the alumina concentration in the ion gels.

*^{2} Alumina [vol%] is concentration for the whole solution.

Table S2 Amount of reagent used for rod-shaped alumina/$[C_4mim][TFSI]$/Ethyl acetate dispersion.

IL $[C_4mim][TFSI]$	EA dispersed alumina*^{1}	Total EA	Alumina		
[g]	[g]	[mL]	[g]	[wt%]*^{2}	[vol%]*^{3}
3.5	1.2	1.2	0.12	4.1	0.65
3.5	2.4	1.2	0.24	7.9	1.3
3.5	3.6	1.2	0.36	12	1.9

*^{1} Alumina concentration in EA dispersed alumina is 10 wt%.

*^{2} Alumina [wt%] corresponds to the alumina concentration in the ion gels.

*^{3} Alumina [vol%] is concentration for the whole solution.

Table S3 Amount of reagent used for spherical alumina/PIL DN ion gels with different alumina concentration.

Monomer	Cross-linking agent	Initiator	IL	Total		Alumina	
$[C_2vim][TFSI]$	$[(Vim)_2C_4][TFSI]_2$	Irgacure2959	$[C_4mim][TFSI]$	EA			
[g]	[g]	[g]	[g]	[mL]	[g]	[wt%]	
3.0	0.021	0.0016	3.5	1.2	0	0	
3.0	0.021	0.0016	3.5	1.2	0.12	4.1	
3.0	0.021	0.0016	3.5	1.2	0.18	6.0	
3.0	0.021	0.0016	3.5	1.2	0.24	7.9	
3.0	0.021	0.0016	3.5	1.2	0.30	10	
3.0	0.021	0.0016	3.5	1.2	0.36	12	
3.0	0.021	0.0016	3.5	1.2	0.42	14	

Table S4 Amount of reagent used for rod-shaped alumina/PIL DN ion gels with different alumina concentration.

Monomer	Cross-linking agent	Initiator	IL	EA dispersed alumina[1]	Total	Alumina	
$[C_2vim][TFSI]$	$[(Vim)_2C_4][TFSI]_2$	Irgacure2959	$[C_4mim][TFSI]$		EA		
[g]	[g]	[g]	[g]	[g]	[mL]	[g]	[wt%]
3.0	0.021	0.0016	3.5	1.2	1.2	0.12	4.1
3.0	0.021	0.0016	3.5	1.8	1.2	0.18	6.0
3.0	0.021	0.0016	3.5	2.4	1.2	0.24	7.9
3.0	0.021	0.0016	3.5	3.0	1.2	0.30	10
3.0	0.021	0.0016	3.5	3.6	1.2	0.36	12
3.0	0.021	0.0016	3.5	4.2	1.2	0.42	14

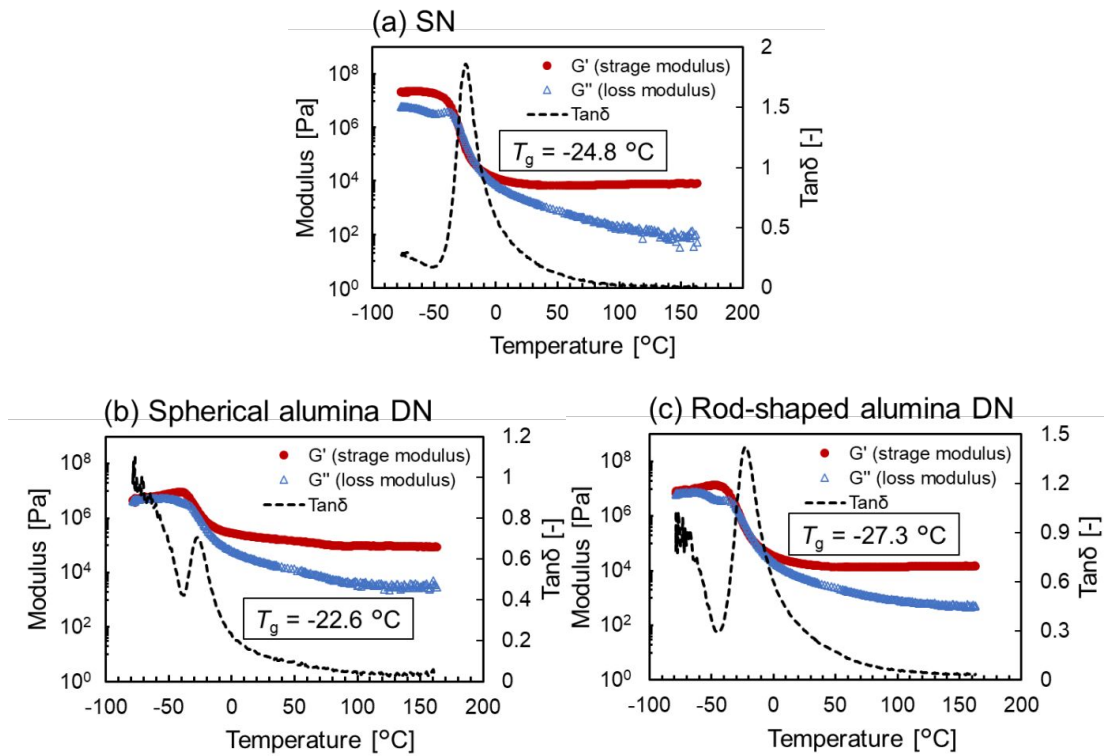[1] Alumina concentration in EA dispersed alumina is 10 wt%.

Figure S3 Oscillatory shear temperature-sweep viscoelasticity measurements of (a) PIL SN, (b) spherical alumina/PIL DN, and (c) rod-shaped alumina/PIL DN ion gels.
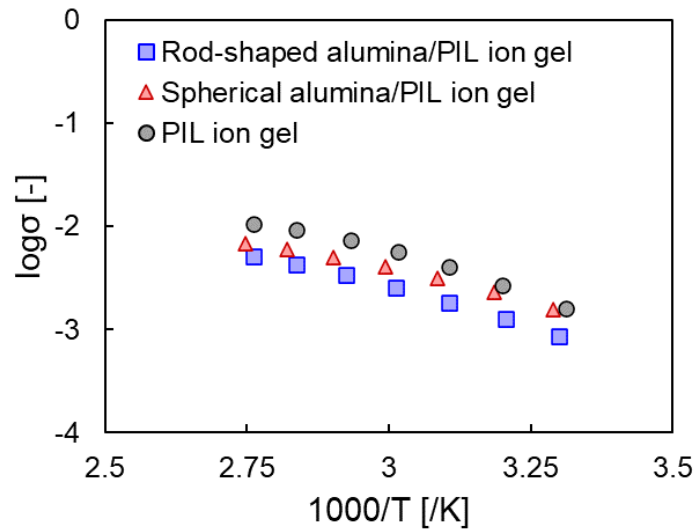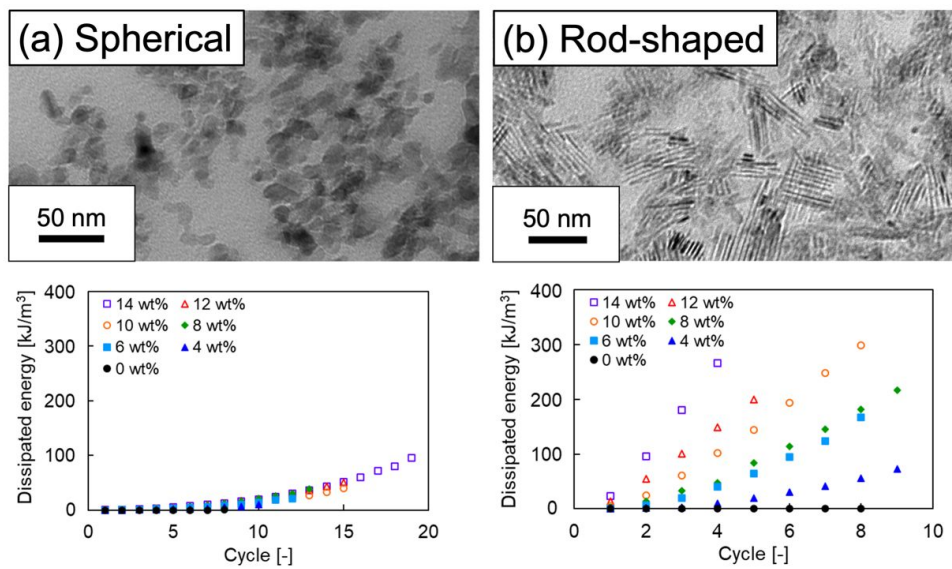

Figure S4 Ionic conductivity (σ) of PIL DN ion gels with different shapes of alumina and PIL SN ion gel.

Table of Contents

The mechanical properties of alumina/poly(ionic liquid) double network ion gels can be controlled by the aggregation structures of nanoparticles.